KSÜ Tarım ve Doğa Derg 27 (Ek Sayı 2), 287-297, 2024
KSU J. Agric Nat 27 (Suppl 2), 287-297, 2024
https://doi.org/10.18016/ksutarimdoga.vi.1470524

Unveiling Anticancer Potential in the Interactions of Melittin Peptides with CD147 Receptor: A Structural and Functional Analysis of Ligand-Target Interactions

Barış DENK[1]✍
[1]Afyon Kocatepe University, Faculty of Veterinary Medicine, Biochemistry Department, Afyonkarahisar, Türkiye
[1]https://orcid.org/0000-0002-7586-0895
✉: bdenk@aku.edu.tr

ABSTRACT

In this study, the anticancer potential of melittin (MLT) peptides interacting with the CD147 receptor was investigated through *in silico* structural and functional analyses. The interaction between the transmembrane glycoprotein CD147 and cyclophilin A (CypA) activates signaling pathways crucial in cancer pathology. This study focused on the potential of melittin peptides to inhibit this interaction. Structures of the CD147 receptor and melittin peptides were obtained from the Protein Data Bank (PDB), including the three-dimensional structure of the Ig1 domain of CD147 (PDB ID: 5XF0) and melittin structures (PDB IDs: 2MLT, 6O4M, 3QRX, 8AHT, and 8AHS). Validated ligand structures were acquired through X-ray crystallography. Receptor-ligand interactions and anticancer activity were evaluated using the ClusPro2.0 molecular docking server, AnciCP2.0 and ENNAACT anticancer analysis servers, ProtScale hydrophobicity analysis, PDBSum amino acid interaction analysis, and PRODIGY thermodynamic stability analysis tools. Molecular docking simulations analyzed receptor-ligand interactions, emphasizing the role of hydrophobic interactions. Structural analysis revealed variability in peptide quality, with 2MLT demonstrating favorable attributes while 3QRX exhibited weak integrity. Anticancer analysis servers indicated that 2MLT and 3QRX, exhibiting similar binding patterns with 5XF0 and CD147/CypA, may demonstrate potential anticancer activity. Specifically, non-bonded interactions involving Gly181 and Arg201 in the 5XF0-2MLT complex and non-bonded interactions involving Pro180, Gly181, and Arg201 in the 5XF0-3QRX complex were highlighted, resembling the interaction pattern of CD147/CypA. Therefore, the importance of understanding molecular interactions and guiding drug discovery through structural examinations and computational analyses was emphasized, providing insights into the anticancer effects and drug design implications of these complexes; moreover, further research into their structural determinants and therapeutic potentials is critically essential for biomedical applications.

Biochemistry

Research Article

Article History
Received : 18.04.2024
Accepted : 07.11.2024

Keywords
Anti-cancer peptides
CD147
Cyclophilin A
Melittin
Molecular docking

Melittin Peptitlerinin CD147 Reseptörü ile Etkileşimindeki Antikanser Potansiyeli: Ligand-Reseptör Etkileşiminin Yapısal ve Fonksiyonel Analizi

ÖZET

Bu araştırmada, antikanser etkileriyle bilinen melittin (MLT) peptitlerinin CD147 reseptörüyle etkileşimlerinin antikanser potansiyeli *in silico* yapısal ve işlevsel analizlerle araştırılmıştır. CD147 transmembran glikoproteini ve siklofilinA (CypA) etkileşimi, kanser patolojisinde önemli olan sinyal yollarını aktive eder. Bu çalışmada, melittin peptitlerinin bu etkileşimi engelleme potansiyeli üzerinde durulmuştur. CD147 reseptör yapısı ve melittin peptit yapıları Protein Veri Bankası'ndan (PDB) temin edilmiş olup; bunlar arasında CD147'nin Ig1 alanının üç boyutlu yapısı (PDB No: 5XF0) ve melittin yapıları (PDB No: 2MLT, 6O4M, 3QRX, 8AHT ve 8AHS) bulunmaktadır. PDB tarafından onaylanmış ligand yapıları X-ışını

Biyokimya

Araştırma Makalesi

Makale Tarihçesi
Geliş Tarihi : 18.04.2024
Kabul Tarihi : 07.11.2024

Anahtar Kelimeler
Antikanser peptitler
CD147
Melittin

kırınımı ile elde edilmiştir. ClusPro2.0 moleküler bağlanma sunucusu, AnciCP2.0 ve ENNAACT antikanser analiz sunucuları, ProtScale hidrofobisite analiz, PDBSum aminoasit etkileşim analiz ve PRODIGY termodinamik stabilite analiz araçları kullanılarak reseptör-ligand etkileşimleri ve antikanser aktivite değerlendirildi. Moleküler bağlanma simülasyonları reseptör-ligand etkileşimlerini analiz etmiş ve hidrofobik etkileşimlerin rolünü vurgulamıştır. Yapısal analiz, peptit kalitesinde değişkenlikleri göstermiş; 2MLT olumlu özellikler sergilerken, 3QRX'in zayıf bütünlük gösterdiği tespit edilmiştir. Antikanser analiz sunucuları 5XF0 ve CD147/CypA ile benzer bağlanma desenleri sergileyen 2MLT ve 3QRX'in her ikisinin de potansiyel antikanser aktivitesi gösterebileceğini ortaya koymuştur. Özellikle 5XF0-2MLT kompleksindeki Gly181 ve Arg201 ile bağsız etkileşimler, 5XF0-3QRX kompleksindeki Pro180, Gly181 ve Arg201 ile bağsız etkileşimler çalışmamızda ortaya konularak CD147/CypA etkileşim şekline benzerliğine dikkat çekilmiştir. Bu nedenle, moleküler etkileşimlerin anlaşılması ve ilaç keşfini yönlendirmenin önemi, yapısal incelemeler ve hesaplamalı analizlerin vurgulanarak, bu komplekslerin antikanser etkileri ve ilaç tasarımı üzerindeki etkilerine dair bilgiler sunulmuştur; ayrıca, bu yapısal belirleyicilerin ve terapötik potansiyellerinin ileri araştırmaları, biyomedikal uygulamalar için kritik öneme sahiptir.

Moleküler bağlanma
Siklofilin A

Atıf Şekli: Melittin Peptitlerinin CD147 Reseptörü ile Etkileşimindeki Antikanser Potansiyeli: Ligand-Reseptör Etkileşiminin Yapısal ve Fonksiyonel Analizi. *KSÜ Tarım ve Doğa Derg 27*(Ek Sayı 2), 287-297. https://doi.org/10.18016/ksutarimdoga.vi.1470524

To Cite : Unveiling Anticancer Potential in the Interactions of Melittin Peptides with CD147 Receptor: A Structural and Functional Analysis of Ligand-Target Interactions. *KSU J. Agric Nat 27* (Suppl 2), 287-297. https://doi.org/10.18016/ksutarimdoga.vi.1470524

INTRODUCTION

Cancer remains a formidable challenge in medical science, with treatment strategies continuously evolving to improve patient outcomes. Despite advancements in cancer therapy, treatment failures still occur due to factors like tumor heterogeneity and resistance mechanisms. Researchers are exploring innovative approaches to combat these challenges, including animal venoms. Venoms, such as those from snakes, bees, and scorpions, contain bioactive compounds that have shown potential in targeting cancer cells with precision. These venom-derived agents can inhibit protein synthesis, induce apoptosis, and disrupt angiogenesis, offering a complementary strategy to conventional treatments. The anticancer effectiveness of animal venoms is attributed to their ability to target cancer cells while minimizing toxicity to normal tissues selectively, thus presenting a promising avenue for enhancing the efficacy of cancer therapeutics (Chaisakul et al., 2016; Gomes et al., 2010; Li et al., 2018; Roy & Bharadvaja, 2021; Sjakste & Gajski, 2023).

Melittin is a potent peptide that is the main component of honeybee (Apis mellifera) venom, constituting about 40–60% of its dry weight (Memariani et al., 2019). It is a cationic amphiphilic peptide known for its diverse biological activities, including antimicrobial, antiviral, and anti-inflammatory effects (Tiwari et al., 2022). Notably, melittin has garnered attention for its anticancer properties. It has been shown to exert antitumor effects by disrupting cell membranes, inhibiting cell growth by interfering with the cell cycle, and inducing apoptosis and necrosis in cancer cells (Daniluk et al., 2022; Huang et al., 2016). Melittin's ability to selectively target cancer cells while sparing normal cells makes it a promising candidate for enhancing the efficacy of traditional cancer therapies (Pandey et al., 2023).

Melittin, a water-soluble peptide from bee venom, has garnered attention for its potential in cancer therapy. It exhibits direct cytotoxic effects on cancer cells and modulates immune responses. Studies have shown that melittin can induce cell cycle arrest and apoptosis, regulate pathways involved in metastasis, angiogenesis, and inflammation, and interact with signaling molecules like Bax, Bcl-2, caspases, and NF-kB. Its ability to inhibit growth and induce apoptosis has been enhanced when delivered in niosomes, making it a promising candidate for cancer treatment. Recent research focuses on improving melittin's selectivity and reducing its toxicity through nanotechnology and combination with conventional drugs (Haque et al., 2023; Pandey et al., 2023).

CD147, or EMMPRIN or basigin, is a transmembrane glycoprotein extensively implicated in cancer progression. Found in various human tumors, CD147 plays a multifaceted role by stimulating the secretion

of matrix metalloproteinases (MMPs) and cytokines. It modulates cellular processes such as proliferation, apoptosis, migration, metastasis, and differentiation, particularly in hypoxic environments. CD147 expression is closely associated with tumor invasion, metastasis, and angiogenesis, rendering it a significant biomarker for cancer prognosis and diagnosis. Additionally, CD147 is a promising therapeutic target, with monoclonal antibodies against it showing potential efficacy, notably in treating hepatocellular carcinoma (Huang et al., 2023; Xiong et al., 2014).

This glycoprotein is notably overexpressed in a broad spectrum of aggressive human cancers, spanning from central nervous system tumors to those of the head and neck, breast, lung, gastrointestinal tract, genitourinary system, skin, and hematological and musculoskeletal systems. Its pivotal role extends to cancer cell proliferation, survival, angiogenesis, metabolic reprogramming, immune evasion, invasion, and metastasis (Nyalali et al., 2023).

The interaction between Cyclophilin A (CypA) and CD147 plays a pivotal role in cancer development. CypA, with its peptidyl-prolyl cis-trans isomerase activity, binds to CD147, influencing multiple cellular functions and activating downstream signaling pathways crucial in cancer pathology. This interaction is associated with increased tumor growth, metastasis, therapeutic resistance, and poor patient prognosis. Studies using The Cancer Genome Atlas (TCGA) database have shown a significant correlation between the overexpression of CypA and CD147 and advanced cancer stages and lower survival rates. Consequently, the CypA/CD147 axis is considered a promising target for anticancer therapy, with the potential to improve treatment outcomes (Bakhtiyari et al., 2023; Han & Jung, 2022; Nyalali et al., 2023; Xiong et al., 2014).

This study aims to investigate the anticancer potential inherent in the interactions between melittin peptides and the CD147 receptor, providing a comprehensive structural and functional analysis of ligand-target interactions. The study aims to elucidate the structural determinants influencing their biological activity through detailed examination and comparison of the structural properties of various melittin peptides and their binding affinities with the CD147 receptor. Additionally, the study explores the role of hydrophobic interactions in forming and stabilizing receptor-ligand complexes, shedding light on the thermodynamic stability of these interactions under different temperature conditions. Computational tools are utilized in molecular docking studies to reveal the in silico structures of receptor-ligand complexes, where receptors consist of proteins and ligands may consist of another protein or small molecule (Oner et al., 2024), and to assess the potential anticancer properties of the examined ligands, providing valuable insights into their therapeutic potential. Overall, this study aims to contribute to the existing knowledge by providing insights into the interactions between melittin peptides and the CD147 receptor, shedding light on their structural and functional aspects.

MATERIAL and METHODS

The Protein Data Bank (PDB), a database storing the structures and related information of biological macromolecules, was utilized to select materials for the research. The molecule structures corresponding to the three-dimensional structure of the Ig1 domain of CD147 with PDB ID 5XF0 (Jin et al., 2018), as well as the structures with PDB IDs 2MLT, 6O4M, 3QRX, 8AHT, and 8AHS, represent melittin, one of the most essential toxins of Apis mellifera. The ligand structures, excluding the receptor structure 5XF0, were validated by depositors using X-ray diffraction and submitted to the Worldwide Protein Data Bank (wwPDB). It is evident from the publicly released X-ray Structure Validation Reports that they are valid PDB entries. As of the date of the study (2024), 13 entries related to melittin were identified on the official website of the PDB: https://www.rcsb.org/. NMR-based structures for ligands were excluded from this study, focusing solely on the five entries obtained through X-ray diffraction methods. This decision was made due to the limited number of NMR-resolved structures available in the PDB (three entries) and the lack of comparability with X-ray crystallographic structures, as normalized real-space R-value (RSRZ) outliers do not apply to NMR. Consequently, a comparative analysis of CD147 interactions between NMR and X-ray crystallographic structures was deemed outside the scope of this study. The interaction between the receptor and ligand molecules was visualized using the molecular surface method in PyMOL.

The Uniprot PDBsum tool was used to analyze the receptor-ligand complexes' PDB files. This tool enabled the visualization of interactions among polypeptide chains, residues, and atoms, encompassing hydrogen bonds, non-bonded contacts, and salt bridges.

The amino acid sequences of the ligands were obtained from the RCSB Protein Data Bank. Subsequently, sequence-specific parameters, including hydrophobicity, hydropathicity, amphipathicity, hydrophilicity, charge, isoelectric point, and molecular weight were predicted using the AntiCP 2.0 server with default settings (Model 1, SVM threshold: 0.45), as described by Agrawal et al., (Agrawal et al., 2021). The analysis of hydrophobicity was further validated using the ProtScale program from The SIB Swiss Institute of Bioinformatics,

employing the Kyte–Doolittle method with a scoring window size of 3 and assigning a relative weight of 100% to the window edges compared to the window center. To assess the anti-cancer activity of the ligands, the ENNAACT web server was employed, and anti-cancer activity scores were predicted as normalized sigmoid scores ranging from 0 to 1, following the method described by Timmons et al. (Timmons & Hewage, 2021).

The ClusPro 2.0 server (Desta et al., 2020; Kozakov et al., 2013, 2017) was employed for docking purposes, utilizing default settings. Following the completion of the docking process, the resulting receptor-ligand complexes were saved in PDB format as optimized docking models, considering the center scores and the number of members. The receptor 5XF0's A chain was selected for the docking process. In this molecule, 20 conformers were loaded into the PDB, of which the first conformer was used for docking. The ligands 2MLT (in homotetramer form, using the A chain for docking) and 6O4M (in homotetramer form, using the B chain for docking) consist of 26 amino acid residues each, with X-ray diffraction resolutions of 2.00 Å (Eisenberg et al., 1990) and 1.27 Å (Kurgan et al., 2019), respectively. 3QRX (in heterodimer form, using the B chain for docking) consists of 20 amino acid residues with an X-ray diffraction resolution of 2.20 Å (Sosa et al., 2011). 8AHT (in heterohexamer form, using the F chain for docking) consists of 25 amino acid residues with an X-ray diffraction resolution of 2.20 Å (Dürvanger et al., 2023). 8AHS (in heterodimer form, using the C chain for docking) consists of 23 amino acid residues with an X-ray diffraction resolution of 2.48 Å (Dürvanger et al., 2023).

Subsequently, the PDB file containing the receptor-ligand complexes was submitted to the Protein Binding Energy Prediction (PRODIGY) server to assess the strength of protein-protein interactions and their thermodynamic stabilities under specific conditions, including temperatures of 25 °C and 40 °C. This analysis predicted the free energy change (ΔG, kcal.mol^{-1}) and the dissociation constant Kd (M).

Statistical analyses

Each receptor-ligand complex is represented by only a single observation, which limits the options for statistical analysis. Descriptive statistics, including minimum, maximum, and arithmetic mean, have been calculated to summarize the findings. However, the results are purely descriptive, and no statistical tests can be applied without additional data.

RESULTS and DISCUSSION

The limited number of structural models of melittin peptides used in this study constrains the generalizability of the findings across all anticancer mechanisms. Additionally, observed limitations related to the models' structural quality may affect the binding results' reliability. Therefore, considering the limited sample size and structural constraints, these findings should be interpreted with caution.

Upon sorting the ligands' scores obtained from the RCSB PDB, the ranking revealed that 2MLT, 6O4M, 3QRX, 8AHT, and 8AHS were arranged in descending order based on their score magnitude. Accordingly, graphs illustrating the overall measures, including free R-value (Rfree), clash score, Ramachandran outliers percent, sidechain outliers percent, and RSRZ outliers percent for the ligands, are presented in Table 1.

Table 1. Percentile ranks for ligands
Çizelge 1. Ligandlar için yüzdelik sıralamalar

Metric	2MLT	6O4M	3QRX	8AHT	8AHS
Rfree	NA	0,235	0,334	0,265	0,303
Clashscore	2	3	8	3	4
Ramachandran outliers (%)	0	0	1,2	0	0
Sidechain outliers (%)	7,1	0	2,9	0,6	0
RSRZ outliers (%)	0	1,7	4,2	4,8	6,7

The table presents percentile ranks for the ligands, with better values highlighted in shades of green and worse in shades of red. The intensity of the green color indicates a higher degree of improvement, while the intensity of the red color signifies a greater degree of deterioration. The quantitative representation of these values is depicted through blue data bars. This adapted form of percentile rank from RCSB PDB visually represents metrics within the table.

A common characteristic of all selected models was their classification as Hydrophobic-favored models within the ClusPro 2.0 server. The scores and coefficients of these models and those of the other models, including Balanced, Electrostatic-favored, and VdW+Elec, are delineated in Table 2. Additionally, it illustrates the outcomes from the PRODIGY server regarding receptor-ligand docking, presenting the Gibbs free energy (ΔG) and dissociation constant (Kd) metrics to assess the binding affinity and thermodynamic stability of protein-protein interactions under variable temperature conditions. It was discerned that among the receptor-ligand complexes, the 5XF0-8AHT

complex exhibited the most substantial ΔG and binding affinity, indicating a robust interaction. Conversely, the weakest ΔG and binding affinity were identified in the 5XF0-3QRX complex. Moreover, an increase in temperature was correlated with a consistent diminution in binding affinity, congruent with the observed trends in ΔG and binding affinity.

Table 2. Summary of binding properties and interaction characteristics of receptor-ligand complexes from molecular docking simulations in ClusPro 2.0

Çizelge 2. ClusPro 2.0 kullanılarak yapılan moleküler bağlanma simülasyonlarından elde edilen reseptör-ligand komplekslerinin bağlanma özellikleri ve etkileşim karakteristiklerinin özeti

Receptor-Ligand Complex	Cluster/Center	Balanced	Electrostatic-favored	Hydrophobic-favored	VdW+Elec	ΔG [kcal.mol-1]	Kd [M] at 25.0 °C/40.0 °C
5XF0-2MLT	Cluster	8	6	13	0	-9.6	8.4e-08/1.8e-07
	Center	-587.0	-623.9	-807.7	-185.7		
5XF0-6O4M	Cluster	1	8	1	2	-9.4	1.3e-07/2.9e-07
	Center	-584.1	-684.3	-932.6	-153.5		
5XF0-3QRX	Cluster	1	2	6	1	-8.8	3.5e-07/7.2e-07
	Center	-591.3	-597.1	-915.7	-127.8		
5XF0-8AHT	Cluster	3	5	0	5	-10.6	1.7e-08/4.1e-08
	Center	-608.3	-676.6	-854.4	-162.3		
5XF0-8AHS	Cluster	7	5	5	9	-9.8	6.7e-08/1.5e-07
	Center	-588.6	-617.4	-908.2	-141.0		
Total	Mean (Cluster/Center)	4.0/-591.86	5.2/-639.86	5.0/-883.72	3.4/-154.06	-9.64	1.3e-07/2.76e-07
	Minimum (Cluster/Center)	1/-608.3	2/-684.3	0/-932.6	0/-185.7	-10.6	1.7e-08/4.1e-08
	Maximum (Cluster/Center)	8/-584.1	8/-597.1	13/-807.7	9/-127.8	-8.8	3.5e-07/7.2e-07
	SD (Cluster/Center)	3.32/9.55	2.17/38.45	5.15/51.59	3.65/21.96	0.65	1.29e-07/2.63e-07

This table summarizes the receptor-ligand complex analyses derived from molecular docking simulations. The parameters include interaction counts categorized as Balanced, Electrostatic-favored, Hydrophobic-favored, and VdW+Elec, as well as binding energy (ΔG) in kcal/mol and dissociation constants (Kd) at 25.0 °C and 40.0 °C. The Total, Mean, Minimum, Maximum, and Standard Deviation (SD) values are provided for both cluster and center metrics, highlighting the analyzed complexes' binding properties and structural quality.

Table 3 encapsulates the predictive analytics of ligands as procured from the AntiCP 2.0 server, detailing the SVM score of each ligand, descriptors of its aqueous interactions, and its chemical attributes. Table 3 also showcases the forecasted anticancer efficacy of therapeutic peptides, as determined by the ENNAACT server. This includes a comprehensive listing of the ligand's amino acid composition and a normalized sigmoidal probability score (PROB score) from 0 to 1. Trained explicitly on a dataset consisting of 861 anticancer peptides and an equal number of non-anticancer peptides through machine learning techniques, the AntiCP 2.0 server (Agrawal, 2021) conducted anticancer scoring for the ligands. The SVM score for 2MLT reached its maximum level, followed sequentially by 8AHT, 8AHS, and 3QRX. Similarly, the ENNAACT server, trained using neural network algorithms, indicates the notably high potential anticancer activity of 2MLT due to its elevated PROB score, followed in descending order by 8AHT, 8AHS, and 3QRX, a finding corroborated by the AntiCP 2.0 server.

The visualizations involve examining the structural details of the interactions between the 5XF0 receptor and the ligands 2MLT, 6O4M, 3QRX, 8AHT, and 8AHS, revealing their chain structures and specific interactions (Figure 1). This structural examination provided insights into the chain structures and interactions of the receptor-ligand complexes, shedding light on their molecular characteristics and potential binding modes.

Structural analyses of 2MLT revealed four hydrogen bonds formed between Ser204, Glu118, and Glu17 residues of 5XF0 and Lys23 and Arg24 residues of 2MLT, accompanied by three salt bridges linking Glu118 and Glu177 residues of 5XF0 with Arg24 and Lys21 residues of 2MLT. Moreover, 79 non-bonded contacts were observed among different amino acids.

Table 3. Predictive analytics of ligands and forecasted anticancer efficacy from AntiCP 2.0 and ENNAACT servers.

Çizelge 3. Ligandların tahmini analizi ve AntiCP 2.0 ve ENNAACT sunucularından öngörülen antikanser etkinliklerinin tahmini.

ID	Seq.	SVM	Hpho.	Hpat.	Amph.	Hphl.	Ch.	pI	Mw	PROB
2MLT, 6O4M	GIGAVLKVLTTGLPALISWIKRKRQQ	1.0	-0.08	0.27	0.71	-0.20	5.0	12.03	2847.91	0.997
3QRX	IGAVLKVLTTGLPALISWIK	0.64	0.18	1.37	0.37	-0.72	2.0	10.02	2093.95	0.905
8AHT	GIGAVLKVLTTGLPALISWIKRKRQ	0.93	-0.06	0.42	0.69	-0.21	5.0	12.03	2719.76	0.995
8AHS	IGAVLKVLTTGLPALISWIKRKR	0.84	-0.04	0.63	0.69	-0.24	5.0	12.03	2534.54	0.990
Total	Mean	0.85	0.00	0.67	0.62	-0.34	4.25	11.53	2549.04	0.97
	Minimum	0.64	-0.08	0.27	0.37	-0.72	2.00	10.02	2093.95	0.91
	Maximum	1	0.18	1.37	0.71	-0.20	5.00	12.03	2847.91	1.00
	SD	0.135	0.105	0.423	0.142	0.218	1.299	0.870	285.39	0.039

Abbreviations: Seq. (Sequence of ligand); SVM (Support Vector Machine score); Hpho. (Hydrophobicity); Hpat. (Hydropathicity); Amph. (Amphipathicity); Hphl. (Hydrophilicity); Ch (Charge); pI (Isoelectric Point); Mw (Molecular Weight); PROB (Normalized Sigmoidal Probability Score). The Total, Mean, Minimum, Maximum, and Standard Deviation (SD) values are provided for analyzed complexes.

Similarly, for 6O4M, five hydrogen bonds involving Glu114, Glu120, Met123, and Asn152 residues of 5XF0 and Arg24, Lys23, Lys21, and Thr10 residues of 6O4M were identified, along with three salt bridges connecting Glu114, Glu120, and Glu168 residues of 5XF0 with Arg24, Lys23, and Lys21 residues of 6O4M. Additionally, 70 non-bonded contacts were noted among various amino acids. Furthermore, structural analysis of 3QRX revealed three hydrogen bonds between Asp144, Glu177, and Arg201 residues of 5XF0 and Trp19, Lys7, and Val8 residues of 3QRX, along with one salt bridge between Glu177 residue of 5XF0 and Lys7 residue of 6O4M. In addition, 60 non-bonded contacts were identified among different amino acids. Moreover, for 8AHT, six hydrogen bonds formed between Glu114, His115, Asn152, Val160, and Glu172 residues of 5XF0 and Lys7, Lys23, and Lys21 residues of 8AHT, accompanied by two salt bridges linking Glu114 and Glu172 residues of 5XF0 with Lys7 and Lys21 residues of 8AHT. Besides, 67 non-bonded contacts were observed among various amino acids. Lastly, structural analysis of 8AHS unveiled five hydrogen bonds involving Gln100, Met123, Arg166, and Glu168 residues of 5XF0 and Leu9, Lys23, and Leu16 residues of 8AHS, along with one salt bridge between Glu168 residue of 5XF0 and Lys23 residue of 8AHS. Additionally, 69 non-bonded contacts were noted among different amino acids.

According to the results presented by the PDBsum server regarding the interactions between the receptor and ligands, various bonding characteristics among residues have been identified. For the 5XF0-2MLT interaction, hydrogen bonds were found to have lengths ranging from a minimum of 2.73 Å to a maximum of 2.85 Å. In comparison, salt bridges ranged from a minimum of 2.59 Å to a maximum of 2.76 Å, and non-bonded contacts ranged from a minimum of 2.56 Å to a maximum of 3.89 Å. In the case of the 5XF0-6O4M interaction, hydrogen bonds ranged from a minimum of 2.59 Å to a maximum of 3.30 Å, salt bridges ranged from a minimum of 2.48 Å to a maximum of 2.75 Å, and non-bonded contacts ranged from a minimum of 2.48 Å to a maximum of 3.90 Å. Regarding the 5XF0-3QRX interaction, hydrogen bonds had lengths ranging from a minimum of 2.48 Å to a maximum of 2.91 Å, with the salt bridge length being 2.48 Å, and non-bonded contacts ranging from a minimum of 2.48 Å to a maximum of 3.88 Å. For the 5XF0-8AHT interaction, hydrogen bonds ranged from a minimum of 2.47 Å to a maximum of 2.77 Å, salt bridges ranged from a minimum of 2.47 Å to a maximum of 2.58 Å, and non-bonded contacts ranged from a minimum of 2.47 Å to a maximum of 3.88 Å. Lastly, in the 5XF0-8AHS interaction, hydrogen bonds had lengths ranging from a minimum of 2.48 Å to a maximum of 3.28 Å, with the salt bridge length being 2.48 Å, and non-bonded contacts ranged from a minimum of 2.48 Å to a maximum of 3.88 Å.

The hydrophobicity indices of the ligands were ascertained using the Kyte–Doolittle scale via the ProtScale tool, as depicted in Figure 2. Based on this scale, the hydrophobicity values observed for 2MLT and 6O4M are significantly elevated. Due to the identical sequences of these peptides, hydrophobicity values are presented in a single graph. Similarly, it is observed that the other peptides exhibit high hydrophobicity, attributed to their similar sequences.

The 2MLT melittin peptide was resolved using X-ray diffraction, with a resolution of 2.00 Å. Although the Rfree value was not specified, a clash score value of 2 indicates a low clash score. The peptide, with a Ramachandran outlier percent of 0%, generally falls within acceptable torsion angle limits; however, the sidechain outlier value of 7.1% suggests some sidechains may have abnormal conformations.

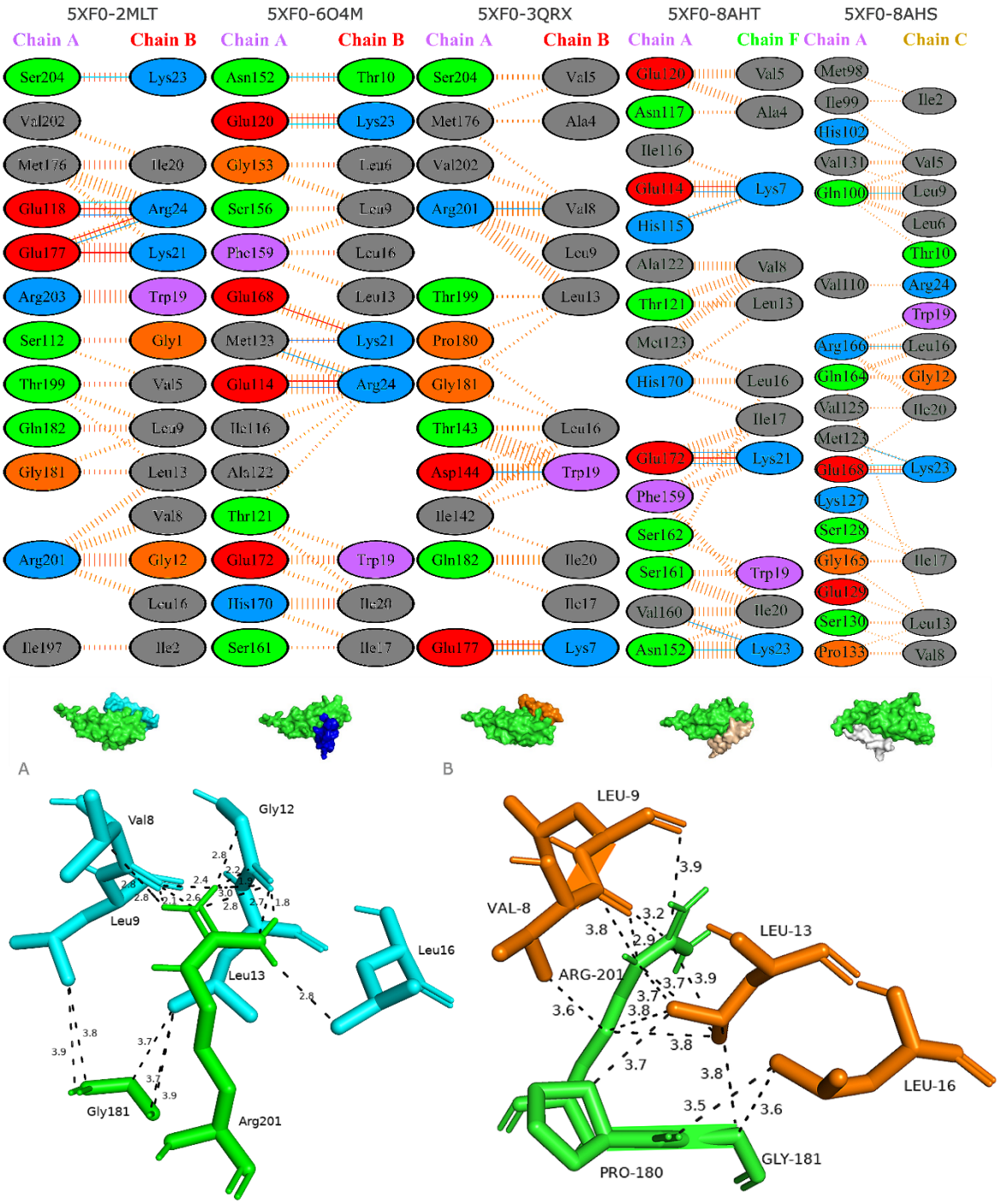

Figure 1. Visualization of interactions between the 5XF0 receptor A chain and ligands via PDBsum and PyMOL

Note. The interactions between the A chain of the 5XF0 receptor and various chains of the ligands are visualized in PDBsum. Discrete vertical red lines represent non-bonded contacts, horizontal red lines denote salt bridges, and horizontal blue lines indicate hydrogen bonds. Using PyMOL software, the interactions are further illustrated, with the receptor depicted in green and the ligands in cyan, blue, orange, wheat, and white. Panel A focuses on the interactions between 5XF0 (green) and 2MLT (cyan), indicating distances in angstroms (Å) with dashed lines. Panel B highlights interactions between 5XF0 (green) and 3QRX (orange), also showing distances in Å with dashed lines.

Şekil 1. 5XF0 reseptörü A zinciri ile ligandlar arasındaki etkileşimlerin PDBsum ve PyMOL ile görselleştirilmesi

Not. 5XF0 reseptörünün A zinciri ile ligandların çeşitli zincirleri arasındaki etkileşimler PDBsum'da görselleştirilmiştir. Ayrık dikey kırmızı çizgiler bağsız etkileşimleri, yatay kırmızı çizgiler tuz köprülerini ve yatay mavi çizgiler hidrojen bağlarını gösterir. PyMOL yazılımı kullanılarak etkileşimler, yeşil renkle gösterilen reseptör ve camgöbeği, mavi, turuncu, buğday ve beyaz ligandlar ile daha ayrıntılı olarak gösterilmektedir. Panel A, 5XF0 (yeşil) ve 2MLT (camgöbeği) arasındaki etkileşimlere odaklanır ve mesafeleri kesikli çizgilerle angstrom (Å) cinsinden göstermektedir. Panel B, 5XF0 (yeşil) ve 3QRX (turuncu) arasındaki etkileşimleri vurgulamakta ve ayrıca mesafeleri kesikli çizgilerle Å cinsinden göstermektedir.

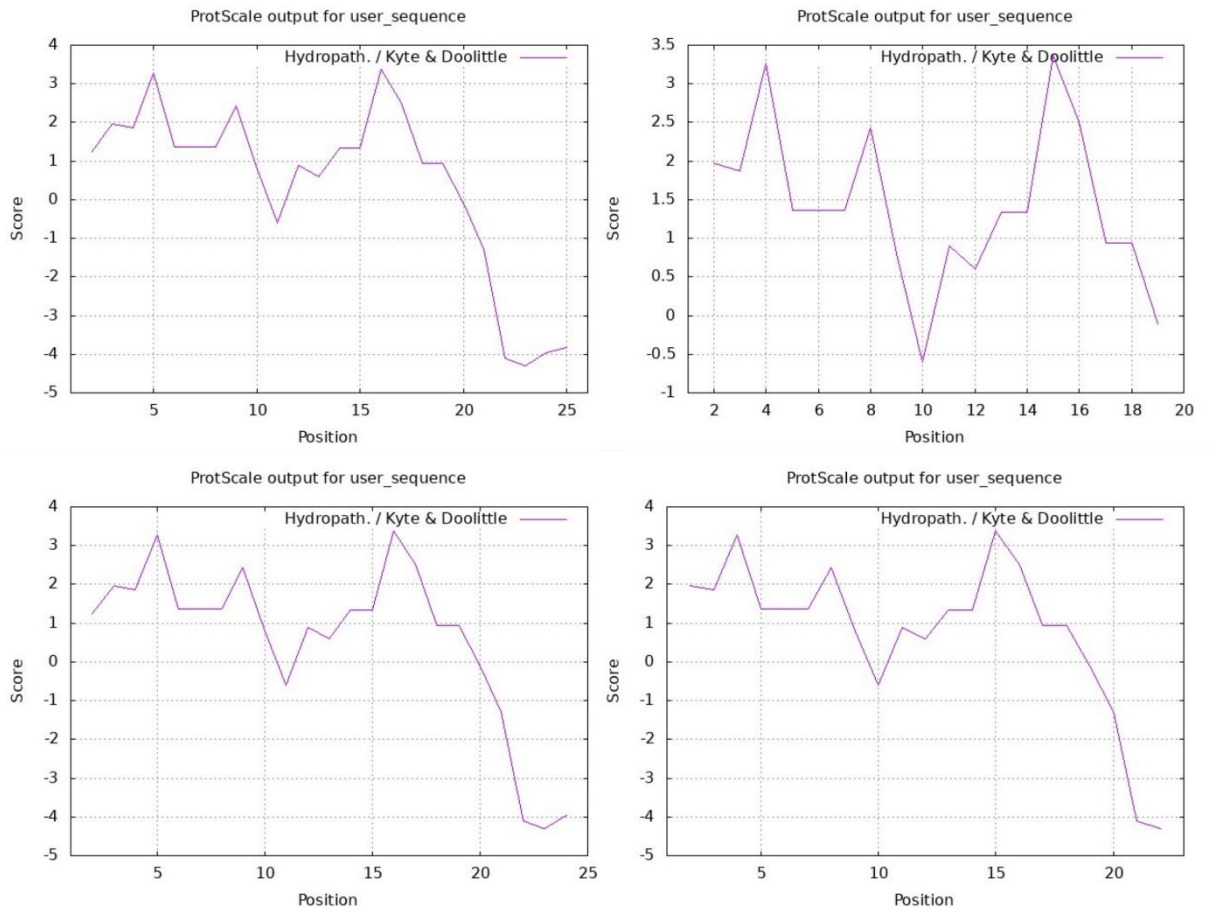

Figure 2. Assessment of ligand hydrophobicity using the Kyte-Doolittle scale

Note. The sequences in the images on the upper left correspond to 2MLT and 6O4M, while the sequence on the right pertains to 3QRX. The sequences in the pictures below correspond to 8AHT on the left and 8AHS on the right. The horizontal axis indicates amino acid positions, while the vertical axis illustrates hydrophobicity levels. Positive values denote the presence of hydrophobic amino acids in the peptide sequence.

Şekil 2. Kyte-Doolittle ölçeği kullanarak ligandların hidrofobiklik değerlendirmesi

Not. Üst panelde soldaki resimde gösterilen diziler 2MLT ve 6O4M'ye karşılık gelirken, sağdaki dizi 3QRX'e aittir. Alt paneldeki resimlerde gösterilen diziler solda 8AHT'ye ve sağda 8AHS'ye karşılık gelmektedir. Yatay eksen amino asit konumlarını gösterirken dikey eksen hidrofobiklik seviyelerini gösterir. Pozitif değerler, peptit dizisinde hidrofobik amino asitlerin varlığını belirtmektedir.

The RSRZ outlier value of 0% generally falls within acceptable limits. The 6O4M melittin peptide has a structural model with a resolution of 1.27 Å and a Rfree value of 0.235, indicating good agreement with experimental data. With a clash score value of 3, the peptide is considered acceptable regarding clashes. The Ramachandran outlier percent of 0% and sidechain outlier value of 0% indicate generally acceptable structural quality; however, the RSRZ outlier value of 1.7% suggests some atoms may have abnormal conformations. The 3QRX melittin peptide has a structural model with a resolution of 2.20 Å but a weak performance fitting experimental data, with an Rfree value of 0.334. Additionally, the peptide has a clash score value of 8, indicating significant problems with clashes. The peptide demonstrates poor structural quality with a Ramachandran outlier percent of 1.2% and a sidechain outlier value of 2.9%. The RSRZ outlier value of 4.2% indicates that some atoms may have abnormal conformations. Finally, the 8AHT and 8AHS melittin peptides have resolutions of 2.20 Å and 2.48 Å, respectively, with Rfree values of 0.265 and 0.303, indicating moderate agreement. However, with a clash score value of 4 and an RSRZ outlier value of 6.7%, the structural quality of 8AHS appears slightly lower compared to 8AHT. Based on the results presented, it can be observed that the structural quality and characteristics of the melittin peptides varied among the complexes analyzed. The 2MLT complex exhibited a relatively favorable structural profile, with low clash scores and acceptable torsion angle limits. In contrast, the 3QRX complex showed weaker performance in fitting experimental data, indicating potential issues with its

structural integrity. However, it should be noted that in terms of molecular binding mode, 3QRX exhibits more remarkable similarity to the CD147/CypA interaction than 2MLT. These findings suggest that the structural properties of the melittin peptides may influence their interactions with the receptor and ultimately impact their biological activity. Further investigations into the structural determinants of these peptides are warranted to elucidate their therapeutic potential and inform drug design strategies.

The selected models were consistently classified as Hydrophobic-favored within the ClusPro 2.0 server, indicating the significant involvement of hydrophobic interactions in both the formation and stabilization of receptor-ligand complexes. Notably, the 5XF0-8AHT complex exhibited the highest ΔG and binding affinity (-10.6 kcal.mol^{-1}; 1.7e-08 M), suggesting a robust and stable interaction. Conversely, the 5XF0-3QRX complex displayed the weakest ΔG and binding affinity (-8.8 kcal.mol^{-1}; 3.5e-07 M), indicative of a comparatively weaker interaction. Furthermore, an increase in temperature correlated with a consistent decrease in binding affinity across the receptor-ligand complexes, aligning with the observed changes in ΔG and binding affinity, thus indicating a temperature-dependent impact on the stability of protein-protein interactions. In summary, these findings underscore the crucial role of hydrophobic interactions in receptor-ligand complex formation. They offer valuable insights into their binding affinity and thermodynamic stability under varying temperature conditions. Such insights contribute significantly to our understanding of the molecular mechanisms governing protein-protein interactions and hold implications for drug discovery and design endeavors.

The AntiCP 2.0 server, trained on a dataset of anticancer and non-anticancer peptides, conducted anticancer scoring for the ligands. The SVM score for 2MLT attained the maximum level (1.0), followed by 8AHT (0.93), 8AHS (0.84), and 3QRX (0.64). Similarly, the ENNAACT server, employing neural network algorithms, indicates the high potential anticancer activity of 2MLT based on its elevated PROB score (0.997), followed by 8AHT (0.995), 8AHS (0.990), and 3QRX (0.905). These findings collectively support the potential anticancer properties of the examined ligands, as highlighted by both computational tools.

The structural examination of molecular complexes has provided insights into receptor-ligand complexes' chain structures and interactions, elucidating their molecular characteristics and potential binding modes. Four and five hydrogen bonds in the 2MLT and 6O4M complexes, respectively, indicate strong interactions with the 5XF0 receptor. Additionally, identifying three salt bridges in these complexes suggests further binding reinforcement. Conversely, three hydrogen bonds and a single salt bridge in the 3QRX complex indicate fewer interactions. The presence of six and five hydrogen bonds in the 8AHT and 8AHS complexes, respectively, demonstrates robust binding between the receptor and ligand. However, the number of salt bridges and non-bonded motifs in these complexes plays a significant role in binding stability and the diversity of specific interactions. These findings contribute to a detailed understanding of the molecular interactions between ligands and receptors, providing a valuable foundation for comprehending the respective ligands' biological activities and therapeutic potentials.

The upregulation of CypA and CD147 in the signaling cascade of malignant cells has been implicated in the initiation and progression of cancer (Han & Jung, 2022; Yurchenko et al., 2010). CypA facilitates signal transduction by forming complexes with Pro180 and Pro211 residues of CD147, with Glu218 playing a pivotal role in this process (Han & Jung, 2022). Recent research has highlighted the regulatory role of Pro180-Gly181 in the CypA/CD147 binding mechanism, identifying Arg201 as a critical residue for this interaction (Yang et al., 2022). Our investigation similarly revealed non-covalent contacts between Gly181 and Leu9, Leu13, and Arg201 with Leu13, Val8, Gly12, and Leu16 in the interaction between 5XF0 and 2MLT, and notably, non-bonded interactions involving Pro180 and Gly181 with Leu13, Leu16, and Arg201 with Val8, Leu9, Leu13 in the case of 3QRX, suggesting specific amino acid interactions independent of chemical bonding. Furthermore, a hydrogen bond between Arg201 and Val8 was identified. While the binding of CypA to CD147 induces conformational changes akin to a molecular chaperone, further exploration of the non-bonded interactions observed with 2MLT and 3QRX warrants investigation in subsequent studies.

The analysis of interactions between the receptor (5XF0) and ligands revealed diverse bonding characteristics across different complexes. Hydrogen bonds, salt bridges, and non-bonded contacts were identified as crucial interaction types. These findings from PDBsum highlight the eclectic nature of interactions between the receptor and ligands, providing valuable insights into their binding mechanisms and potential functional implications.

The hydrophobicity indices obtained using the Kyte-Doolittle scale via the ProtScale tool reveal significant attributes of the ligands under scrutiny. The ligands exhibit elevated hydrophobicity, presumably stemming from their similar sequences. In particular, the sequence 3QRX, which corresponds to IGAVLKVLTTGLPALISWIK, shows a significantly hydrophobic nature, whereas the sequences 2MLT and 6O4M, represented by

GIGAVLKVLTTGLPALISWIKRKRQQ, possess relatively lower hydrophobicity. Additionally, variations in amphipathicity and hydrophilicity properties are observed across different sequences. These observations underscore the hydrophobic nature of the ligands under examination and emphasize the potential ramifications of their hydrophobic properties in diverse biological processes and interactions, warranting further investigation in subsequent analyses.

In conclusion, the analysis of the 3QRX ligand and its interaction with the 5XF0 receptor reveals crucial insights into receptor-ligand interactions. Despite structural deficiencies such as clashes and abnormal conformations, 3QRX exhibits a molecular binding mode that closely resembles the CD147/CypA interaction, suggesting potential similarities in their biological mechanisms. Furthermore, the notably hydrophobic nature of the 3QRX sequence may influence its interaction with the receptor. However, the 5XF0-3QRX complex demonstrates the weakest binding affinity among the studied complexes, indicating a weaker interaction. These findings emphasize the significance of considering both structural and sequence-based characteristics when assessing the efficacy of receptor-ligand interactions, offering valuable insights into the molecular basis of protein-protein interactions.

CONCLUSION

To summarize, the comprehensive analysis presented in this study sheds light on various aspects of receptor-ligand interactions and their implications. Structural examinations elucidated the complexes' molecular characteristics and binding modes, highlighting the significance of hydrogen bonds, salt bridges, and non-bonded contacts. Computational tools provided insights into the potential anticancer properties of the ligands, with notable variations in hydrophobicity observed across different sequences. The classification of models as Hydrophobic-favored underscores the role of hydrophobic interactions in complex stability. Moreover, temperature-dependent effects on binding affinity emphasize the dynamic nature of protein-protein interactions. These findings deepen our understanding of molecular interactions and provide valuable insights for drug discovery and design efforts in various biomedical applications. Further research into these complexes' structural determinants and therapeutic potentials is warranted to advance our knowledge and facilitate the development of novel therapeutics.

Contribution of Authors

BD: Design, Perform, Analyze, Write and editing, Project Administration.

Conflict of Interests and Ethical Statement

None.

REFERENCES

Agrawal, P., Bhagat, D., Mahalwal, M., Sharma, N., & Raghava, G. P. S. (2021). AntiCP 2.0: an updated model for predicting anticancer peptides. *Briefings in Bioinformatics, 22*(3), bbaa153.

Bakhtiyari, M., Haji Aghasi, A., Banihashemi, S., Abbassioun, A., Tavakol, C., & Zalpoor, H. (2023). CD147 and cyclophilin A: a promising potential targeted therapy for COVID-19 and associated cancer progression and chemo-resistance. *Infectious Agents and Cancer, 18*(1), 20.

Chaisakul, J., Hodgson, W. C., Kuruppu, S., & Prasongsook, N. (2016). Effects of animal venoms and toxins on hallmarks of cancer. *Journal of Cancer, 7*(11), 1571.

Daniluk, K., Lange, A., Pruchniewski, M., Małolepszy, A., Sawosz, E., & Jaworski, S. (2022). Delivery of melittin as a lytic agent via graphene nanoparticles as carriers to breast cancer cells. *Journal of Functional Biomaterials, 13*(4), 278.

Desta, I. T., Porter, K. A., Xia, B., Kozakov, D., & Vajda, S. (2020). Performance and its limits in rigid-body protein-protein docking. *Structure, 28*(9), 1071–1081.

Dürvanger, Z., Juhász, T., Liliom, K., & Harmat, V. (2023). Structures of calmodulin–melittin complexes show multiple binding modes lacking classical anchoring interactions. *Journal of Biological Chemistry, 299*(4).

Eisenberg, D., Gribskov, M., & Terwilliger, T. C. (1990). Melittin. Retrieved from https://doi.org/10.2210/pdb2MLT/pdb

Gomes, A., Bhattacharjee, P., Mishra, R., Biswas, A. K., Dasgupta, S. C., Giri, B., Debnath, A., Gupta, S. Das, Das, T., & Gomes, A. (2010). Anticancer potential of animal venoms and toxins.

Han, J. M., & Jung, H. J. (2022). Cyclophilin A/CD147 interaction: A promising target for anticancer therapy. *International Journal of Molecular Sciences, 23*(16), 9341.

Haque, S., Hussain, A., Joshi, H., Sharma, U., Sharma, B., Aggarwal, D., Rani, I., Ramniwas, S., Gupta, M., & Tuli, H. S. (2023). Melittin: a possible regulator of cancer proliferation in preclinical cell culture and animal models. *Journal of Cancer Research and Clinical Oncology, 149*(19), 17709–17726.

Huang, D., Rao, D., Jin, Q., Lai, M., Zhang, J., Lai, Z., Shen, H., & Zhong, T. (2023). Role of CD147 in the development and diagnosis of hepatocellular carcinoma. *Frontiers in Immunology, 14*, 1149931.

Huang, S., Jianhua, W., Xiaozhong, W., & Chenghong, L. I. (2016). Melittin: A key composition of honey bee venom with diverse

pharmaceutical functions. Paper presented at the *International Conference on Biological Engineering and Pharmacy 2016 (BEP 2016)*, 193–197.

Jin, S., Ding, P., Chu, P., Li, H., Sun, J., Liang, D., Song, F., & Xia, B. (2018). Zn(II) can mediate self-association of the extracellular C-terminal domain of CD147. *Protein & Cell, 9*(3), 310–315. https://doi.org/10.1007/s13238-017-0443-1

Kozakov, D., Beglov, D., Bohnuud, T., Mottarella, S. E., Xia, B., Hall, D. R., & Vajda, S. (2013). How good is automated protein docking? *Proteins: Structure, Function, and Bioinformatics, 81*(12), 2159–2166.

Kozakov, D., Hall, D. R., Xia, B., Porter, K. A., Padhorny, D., Yueh, C., Beglov, D., & Vajda, S. (2017). The ClusPro web server for protein-protein docking. *Nature Protocols, 12*(2), 255–278.

Kurgan, K. W., Kleman, A. F., Bingman, C. A., Kreitler, D. F., Weisblum, B., Forest, K. T., & Gellman, S. H. (2019). Retention of native quaternary structure in racemic melittin crystals. *Journal of the American Chemical Society, 141*(19), 7704–7708.

Li, L., Huang, J., & Lin, Y. (2018). Snake venoms in cancer therapy: past, present and future. *Toxins, 10*(9), 346.

Memariani, H., Memariani, M., Shahidi-Dadras, M., Nasiri, S., Akhavan, M. M., & Moravvej, H. (2019). Melittin: from honeybees to superbugs. *Applied Microbiology and Biotechnology, 103*, 3265–3276.

Nyalali, A. M. K., Leonard, A. U., Xu, Y., Li, H., Zhou, J., Zhang, X., Rugambwa, T. K., Shi, X., & Li, F. (2023). CD147: an integral and potential molecule to abrogate hallmarks of cancer. *Frontiers in Oncology, 13*.

Oner, E., Demirhan, I., Kurutas, EB., & Yalin, S (2024). Investigation of Active Compounds in Propolis Structure Against Sars Cov-2 Main Protease by Molecular Docking Method: In Silico Study. *Journal Of Agriculture and Nature 27*(1), 46–55. https://doi.org/10.18016/ksutarimdoga.vi.1093707.

Pandey, P., Khan, F., Khan, M. A., Kumar, R., & Upadhyay, T. K. (2023). An updated review summarizing the anticancer efficacy of melittin from bee venom in several models of human cancers. *Nutrients, 15*(14), 3111.

Roy, A., & Bharadvaja, N. (2021). Venom-derived bioactive compounds as potential anticancer agents: a review. *International Journal of Peptide Research and Therapeutics, 27*, 129–147.

Sjakste, N., & Gajski, G. (2023). A review on genotoxic and genoprotective effects of biologically active compounds of animal origin. *Toxins, 15*(2), 165.

Sosa, L. del V., Alfaro, E., Santiago, J., Narváez, D., Rosado, M. C., Rodríguez, A., Gómez, A. M., Schreiter, E. R., & Pastrana-Ríos, B. (2011). The structure, molecular dynamics, and energetics of centrin–melittin complex. *Proteins: Structure, Function, and Bioinformatics, 79*(11), 3132–3143.

Timmons, P. B., & Hewage, C. M. (2021). ENNAACT is a novel tool that employs neural networks for anticancer activity classification for therapeutic peptides. *Biomedicine & Pharmacotherapy, 133*, 111051.

Tiwari, R., Tiwari, G., Lahiri, A., Ramachandran, V., & Rai, A. (2022). Melittin: a natural peptide with expanded therapeutic applications. *The Natural Products Journal, 12*(2), 13–29.

Xiong, L., Edwards III, C. K., & Zhou, L. (2014). The biological function and clinical utilization of CD147 in human diseases: a review of the current scientific literature. *International Journal of Molecular Sciences, 15*(10), 17411–17441.

Yang, Z., Zang, Y., Wang, H., Kang, Y., Zhang, J., Li, X., Zhang, L., & Zhang, S. (2022). Recognition between CD147 and cyclophilin A deciphered by accelerated molecular dynamics simulations. *Physical Chemistry Chemical Physics, 24*(31), 18905–18914.

Yurchenko, V., Constant, S., Eisenmesser, E., & Bukrinsky, M. (2010). Cyclophilin–CD147 interactions: a new target for anti-inflammatory therapeutics. *Clinical & Experimental Immunology, 160*(3), 305–317.